Ni x Pb 1− x Nanowire Arrays: Effects of Annealing

ARTICLE *in* THE JOURNAL OF PHYSICAL CHEMISTRY B · OCTOBER 2005

Impact Factor: 3.3 · DOI: 10.1021/jp0519520 · Source: PubMed

8 AUTHORS, INCLUDING:

Guangbin Ji
Nanjing University of Aeronautics & Astronau…
84 PUBLICATIONS **1,512** CITATIONS
SEE PROFILE

Hailin Su
Hefei University of Technology
31 PUBLICATIONS **210** CITATIONS
SEE PROFILE

Tang Shaolong
Nanchang University
58 PUBLICATIONS **608** CITATIONS
SEE PROFILE

Youwei Du
Dalian Maritime University
317 PUBLICATIONS **4,081** CITATIONS
SEE PROFILE

Ni_xPb_{1-x} Nanowire Arrays: Effects of Annealing

Guangbin Ji,*,† Jieming Cao,*,† Fang Zhang,† Guoyue Xu,† Hailin Su,‡ Shaolong Tang,‡ Benxi Gu,‡ and Youwei Du‡

Nanomaterials Research Institute, College of Material Science and Technology, Nanjing University of Aeronautics and Astronautics, Nanjing 210016, People's Republic of China, and National Laboratory of Solid State Microstructure and Department of Physics, Nanjing University, Nanjing 210093, People's Republic of China

Received: April 15, 2005; In Final Form: July 18, 2005

Ni_xPb_{1-x} nanowire arrays were successfully fabricated by AC electrodeposition within the nanopores of ordered porous alumina films prepared by a two-step anodization. Transmission electron microscopy analyses showed that the Ni−Pb nanoarrays are polycrystalline with dimension uniformity around 20 nm in diameter and lengths up to several micrometers. X-ray diffraction results revealed that the face-centered-cubic (fcc) Ni and fcc Pb peaks are detected when the Ni component (x) is below 0.71, indicating that the Ni_xPb_{1-x} nanoarrays do not form metastable phase alloy. Hysteresis loops determined by vibrating sample magnetometer indicated that the Ni_xPb_{1-x} nanoarrays obtained possess obvious magnetic anisotropy, and the perpendicular coercivity was lower than that of pure Ni nanowries before and after annealing. Annealing under magnetic field was carried out to examine the effect of a magnetic field on magnetic properties using an electromagnet field up to 0.3 T.

Introduction

Magnetic nanowire arrays have attracted much interest recently because of their potential application in ultrahigh-density magnetic recording media,[1−4] highly sensitive giant magnetoresistance (GMR) sensors,[5,6] and other applications. Although many different techniques have been employed to synthesize such nanomaterials, among them, template synthesis, pioneered by Martin,[7] has proved to be the one with low cost and high yield. Examples of nanoporous membranes that have been used include polycarbonate membranes, nanochannel array glasses, mesoporous channel hosts, and anodic alumina oxide (AAO) templates. Compared to the other membranes, the AAO template has been proved to be versatile because of its self-organized, cylindrical, uniform holes, of which the size can be readily controlled by properly adjusting the anodizing condition and subsequent procedure.[8] The AAO template is also stable at high temperature and in organic solvents. A number of methods have also been applied to produce the array, such as electroless plating, sol−gel, and chemical vapor deposition. Electrochemical assembly of highly ordered uniform nanoarrays into an AAO template is one of the simplest and most inexpensive methods. The alternating current (AC) electrodepositon into an AAO template has proved to be a simple approach compared to direct current (DC) electrodeposition process because it does require the removal of the Al substrate and the barrier layer of alumina.[9]

In our previous work, we have successfully synthesized magnetic nanowire arrays by electrodeposition into AAO template such as Co,[10] Fe,[11] FeCo,[12] CoPt,[13] and CoPb nanowires.[14] Other research groups also reported the preparation and magnetic properties of nano arrays such as Ni,[15] FeNi,[16] FePt,[17] NiCu,[4,18] CoP,[19] and FeP [20] nanowires. Although there have been numerous publications about magnetic nanowire arrays based on the AAO synthesis, however, only a few studies on heterogeneous ferromagnetic−nonmagnetic alloy nanowire array systems are reported in the literature. Among them, Blythe et al.[21] have fabricated Co−Cu alloy nanowires and presented a preliminary study of their transport properties. Fedosyuk et al.[22] reported on the granular Ag−Co deposited in porous anodic aluminum oxide that exhibited a magnetoresistance effect at room temperature. Wang et al.[23] have fabricated Fe−Ag and Co−Ag nanowire arrays embedded in an AAO template and revealed the variation of the coercivities versus annealing temperature. To our best knowledge, fabrication and magnetic properties of Ni−Pb systems have not been reported so for. Here, we report the first successful synthesis of high-density Ni_xPb_{1-x} nanoarrays with obvious perpendicular anisotropy by AC electrodeposition into AAO template, and the effects of the different annealing conditions and temperatures on magnetic properties have been discussed in detail.

Experimental Section

The AAO templates used for the electrodepositon of Ni_xPb_{1-x} nanowire arrays were prepared using superpure aluminum 99.99% foils. Prior to anodizing, the aluminum foils (20 × 20 × 0.1 mm) were degreased with acetone and annealed in 500 °C for 2 h in the open air in order to obtain homogeneous grains and reduce the defect density in the foils. This process was essential for the formation of highly ordered nanochannels during the subsequent anodization. A mirror surface was achieved by electropolishing in a mixed solution of $HClO_4$ and C_2H_5OH. The ordered porous alumina templates were prepared via a two-step anodizing process. Briefly, the clean aluminum foil was first anodized in 0.3 M H_2SO_4 aqueous solution under a constant voltage of 20 V for 10 h at 0 °C. Subsequently, the alumina was removed in a mixture of phosphoric acid and chromic acid, and the Al foils were anodized again for 2 h under the same conditions as above (temperature, electrolyte concentration, and anodizing voltage). To obtain the AC electrodeposition into the pores, it is highly necessary to previously reduce the alumina barrier thickness at the pore bottom[24] by an

* To whom correspondence should be addressed. E-mail: (J.C.) jmcao@nuaa.edu.cn; (G.J.) gbji@nuaa.edu.cn.
† Nanjing University of Aeronautics and Astronautics.
‡ Nanjing University.

10.1021/jp0519520 CCC: $30.25
Published on Web 08/23/2005

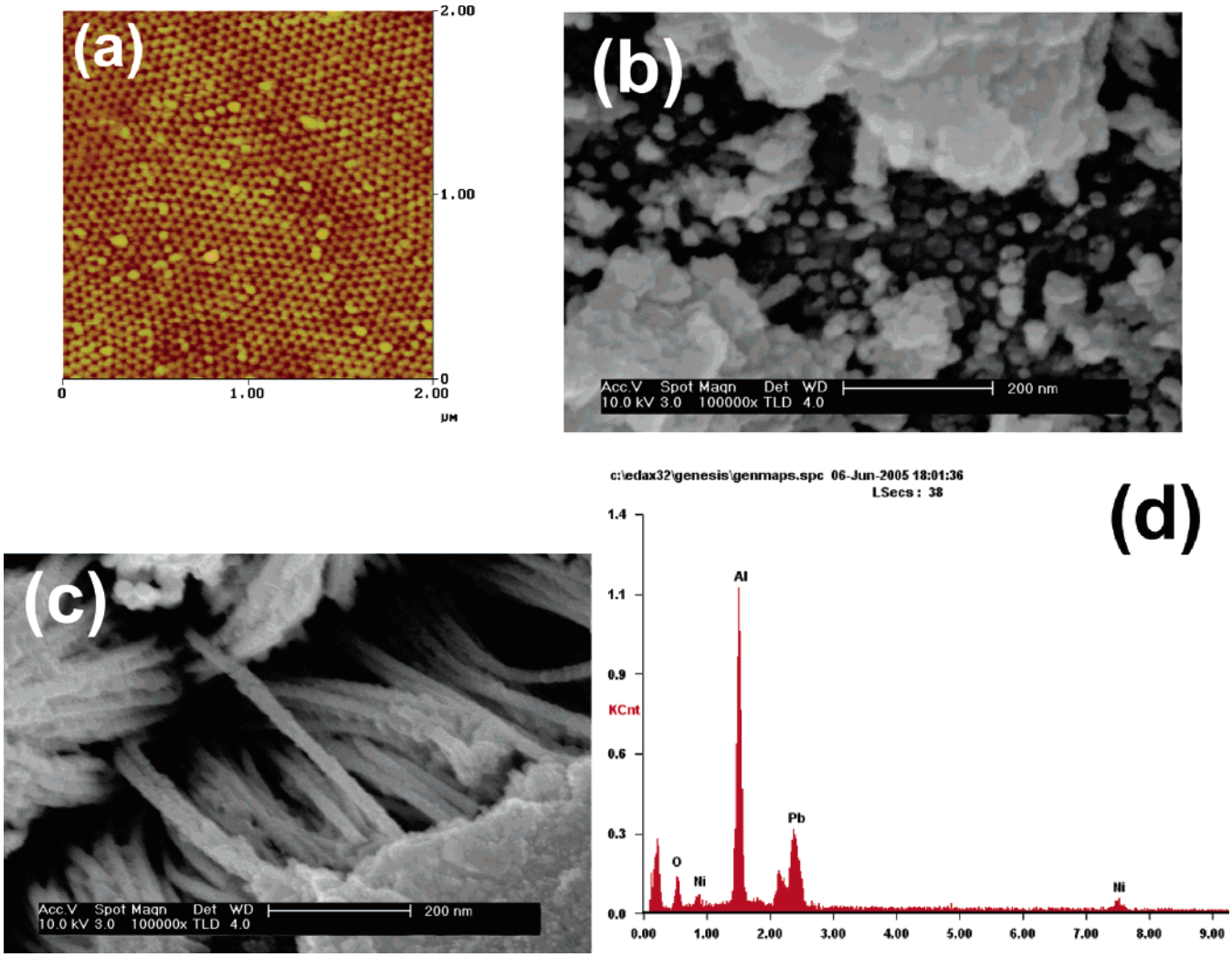

Figure 1. (a) AFM image of AAO template fabricated using a two-step anodized process after chemical etching in phosphoric acid solution. FE-SEM images of the as-deposited Ni−Pb nanowires embedded in the AAO template; (b) top view; (c) several nanowires partly detached from the AAO template; (d) EDAX spectrum of the Ni−Pb nanowire arrays.

appropriate chemical dissolution (0.36 M H_3PO_4, 30 °C), yielding a highly ordered 10 μm thick porous alumina layer containing straight, parallel pores with an average diameter of about 20 nm.

Deposition was carried out at 26 °C with an AC voltage of 16 V, 50 Hz using graphite as counter electrode and AAO template with aluminum plate as working electrode. The deposition time was 20 min. The composition of the Ni_xPb_{1-x} nanowires was analyzed by induction-coupled plasma spectrometer (ICP). To achieve this composition in electrodeposited Ni_xPb_{1-x} nanowires, the relative Ni concentration has to be greatly increased due to the extremely high rate of Pb deposition compared to that of Ni. The electrolyte used to electrodeposit Ni_xPb_{1-x} nanowires had the following composition: 10−30 g/L $Ni(CH_3COO)_2 \cdot 4H_2O$; 1−6 g/L $Pb(CH_3COO)_2 \cdot 3H_2O$; 30 g/L H_3BO_3 with a pH value of 5.5. After electrodeposition, the Ni_xPb_{1-x} ($0.49 \leq x \leq 1$) nanoarrays were annealed for 20 min at different temperatures (300, 400, 500, and 600 °C) under a flowing H_2 atmosphere. To obtain good magnetic properties, a 0.3 T field was applied parallel to the Ni−Pb/Al_2O_3 nanoarrays using an electromagnet. The magnetic field was applied during annealing and cooling.

The magnetic properties were measured by vibrating sample magnetometer (VSM, Lakeshore, Model 7300 series) with the applied field either perpendicular or parallel to the surface of the samples. The AAO templates were characterized by an atomic force microscopy (AFM, Digital Instruments Nanoscope IIIa). The morphology of the Ni−Pb nanowires was observed by field emission scanning electron microscopy (FE-SEM, FEI SIRION 200) with an energy-dispersive X-ray analyzer (EDAX) and transmission electron microscopy (TEM, TECNAI G^2 20 S-TWIN). For the SEM observation, small pieces of AAO with Ni−Pb nanowires sample were eroded by an aqueous solution of 5% H_3PO_4 for 10 min at 30 °C in order to remove the upper part of AAO and then washing with distilled water several times. For the TEM investigation, the AAO/Ni−Pb system was immersed in 1 M NaOH for 10 min at room temperature and dispersed in alcohol, and then a small drop of solution was placed on Cu grids covered with carbon film. The phase structure characterization of Ni−Pb nanoarrays was carried out by X-ray diffraction (XRD) in the 2θ range of 20−80 using Cu Kα X-ray source ($\lambda = 0.154\ 18$ nm) with voltage and current of 40 kV and 100 mA, respectively. For studying the chemical composition of the nanowires, The X-ray photoelectron spectroscopy (XPS, ESCALab MK2) was used with Mg Kα source. The C_{1s} ($E = 284.5$ eV) level served as the internal standard.

Results and Discussion

Figure 1a shows the AFM micrographs of the top view of the AAO templates after chemical etching in phosphoric acid

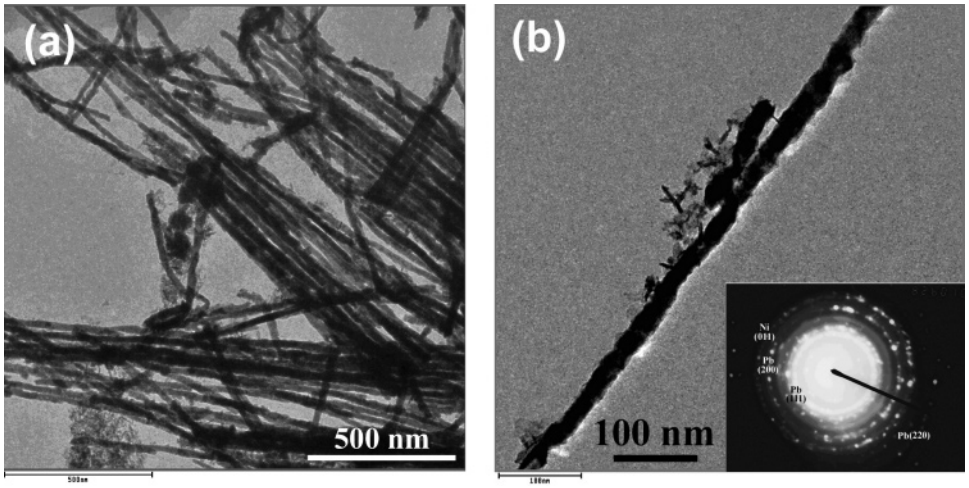

Figure 2. TEM images of the Ni−Pb nanowires with diameter about 20 nm detached from the AAO template: (a) a bundle of nanowires and (b) an isolated nanowire with the inset for the SAED pattern taken from the nanowire.

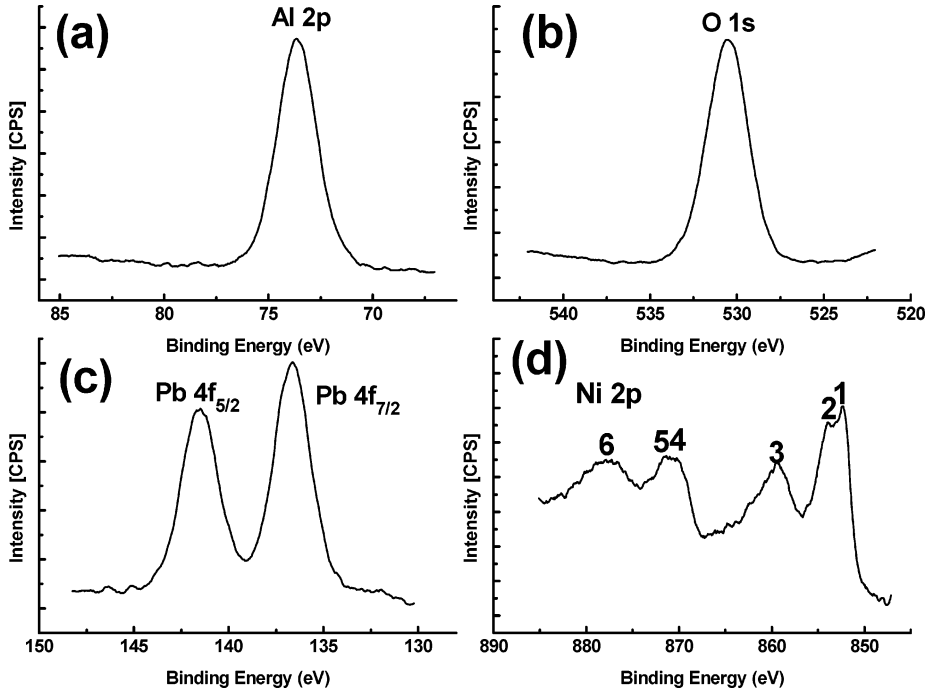

Figure 3. XPS spectra of Al 2p (a), O 1s (b), Pb 4f (c), and Ni 2p (d) core levels for the as-deposited Ni−Pb/Al_2O_3 nanowire arrays.

solution. The perfect hexagonally arranged pore arrays in Figure 1a have identical pore diameters of about 20 nm, and the pore density is about 10^{10}−10^{11} cm^{-2}. The diameter and the interval of the pores are based on the applied voltage. Adjusting the applied voltage and using different electrolytes can be used to prepare AAO templates with different diameters and lengths. Top-view FE-SEM images (Figure 1b) more clearly show that a number of nanowires grew inside the arranged pore arrays of the AAO template.

A typical FE-SEM image of Ni−Pb nanowires is shown in Figure 1c. In this image, the alumina matrix is almost completely dissolved. The nanowire arrays fill the nanochannels uniformly, and the nanowires are apparently continuous. The measured diameter of the nanowires corresponds closely to the pore diameter. The EDAX spectrum (Figure 1d) on the nanowires reveals the presence of only lead, nickel, aluminum, and oxygen. These results clearly indicate that ordered Ni−Pb nanowire arrays deposited inside the channels of the alumina membrane.

The Ni−Pb nanowires after removal of the AAO film, determined by means of TEM shown in Figure 2, indicate that Ni−Pb has been electrodeposited in the nanoholes of the AAO template. Figure 2a presents a bundle of nanowires after dissolving the AAO template. Clearly, the nanowires are both continuous and uniform, with an average diameter of about 20 nm and the length up to several micrometers. Figure 2b shows an isolated Ni−Pb nanowire, where the inset is the corresponding selected-area electron diffraction (SAED) patterns showing that the nanowire is polycrystalline. The lattice plane distances we derived from the diffraction rings of the as-deposited samples fit well to the formula $d = a/\sqrt{h^2+k^2+l^2}$; here h, k, l are the indexes we note in Figure 2b, and a is the lattice constant, which indicates that the Ni−Pb nanowires has face-centered-cubic (fcc) Ni and Pb structures.

The chemical composition of the Ni−Pb nanowires embedded in the AAO template was determined using XPS. The XPS spectra of the Ni−Pb nanowires are shown in Figure 3. The XPS analysis indicates that the sample is composed of Ni, Pb, Al, and oxygen. Figure 3d shows Ni 2p high-resolution XPS spectrum. From the XPS handbook,[25] we know that peak 1 at

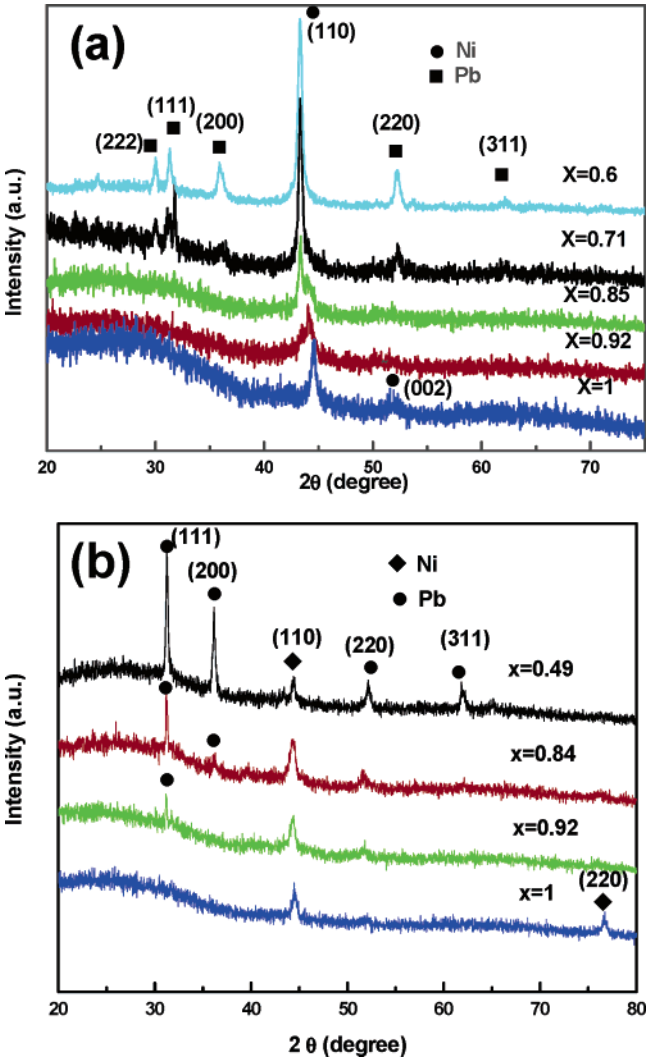

Figure 4. XRD patterns of the Ni_xPb_{1-x} nanowires with different Ni components (a) before and (b) after H_2 annealing.

852.3 eV and peak 2 at 853.9 eV are characteristic of metallic Ni $2p_{3/2}$ and oxidized Ni $2p_{3/2}$ peaks, respectively. Peaks 4 and 5 correspond to metallic Ni $2p_{1/2}$ and oxidized Ni $2p_{1/2}$ peaks, respectively. The main peaks, corresponding to Ni $2p_{3/2}$ and $2p_{1/2}$, respectively, are accompanied by the satellites at higher binding energies (peaks 3 and 6).[26] The above XPS analysis results indicate that the Ni deposit is not a single substance like Pb 4f. Little Ni oxides form during AC electrodeposition.

Figure 4 shows the X-ray diffraction spectra of the Ni_xPb_{1-x} nanowires (with x ranging from 0.49 to 1) before and after H_2 annealing. The XRD measurement shows that all peaks of our as-deposited samples for $x > 0.71$ are consistent with those of fcc Ni. The fcc Pb peaks are observed for $x < 0.71$, indicating the existence of Pb precipitates. One can see that the Ni and Pb diffraction lines are shifted toward lower and higher angles, respectively. We know that the Ni−Pb represents an immiscible pair of materials under equilibrium conditions. However, under nonequilibrium conditions such as quick AC electrodepositon, the Ni−Pb system could form a miscible phase to a certain extent. After annealing, all peaks of our samples are consistent with those of a typical structure fcc Pb and fcc Ni for $x < 0.92$, indicating the recrystallization of the as-prepared samples into fcc Pb and fcc Ni. The crystallite size is determined from the width of the diffraction peaks at half-maximum using Sherrer's formula. The crystallite size is found to range from 8 to 20 nm

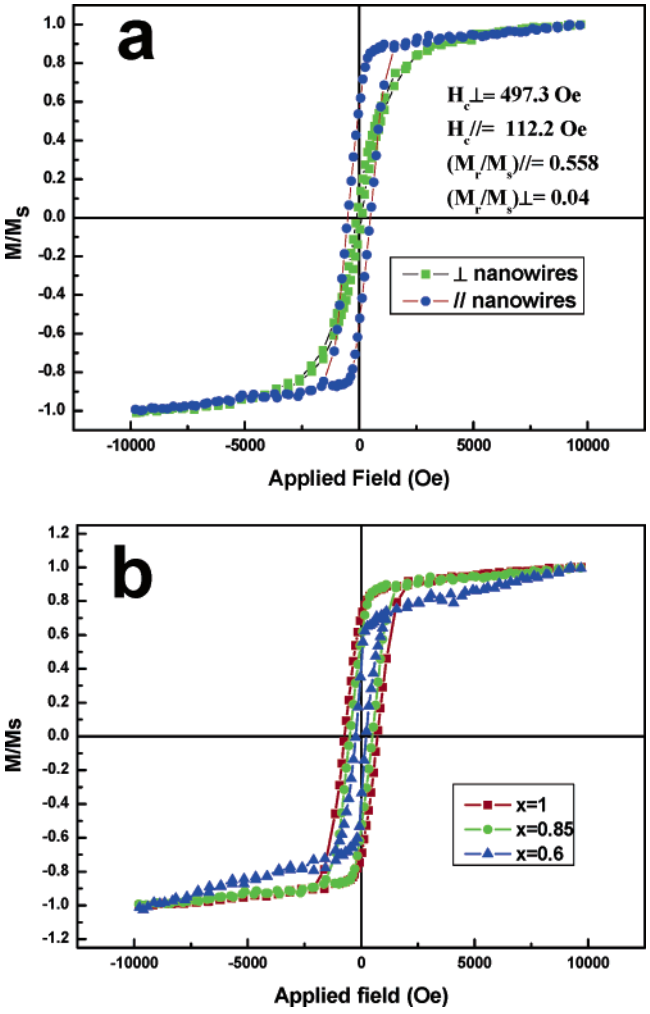

Figure 5. Representative $M-H$ loops of the as-deposited (a) $Ni_{0.85}Pb_{0.15}$ nanowire arrays measured in a magnetic field parallel and perpendicular to nanowires and (b) Ni_xPb_{1-x} ($0.60 < x < 1.0$) nanowire arrays measured in a magnetic field parallel to nanowires at room temperature with the applied field of 10 kOe.

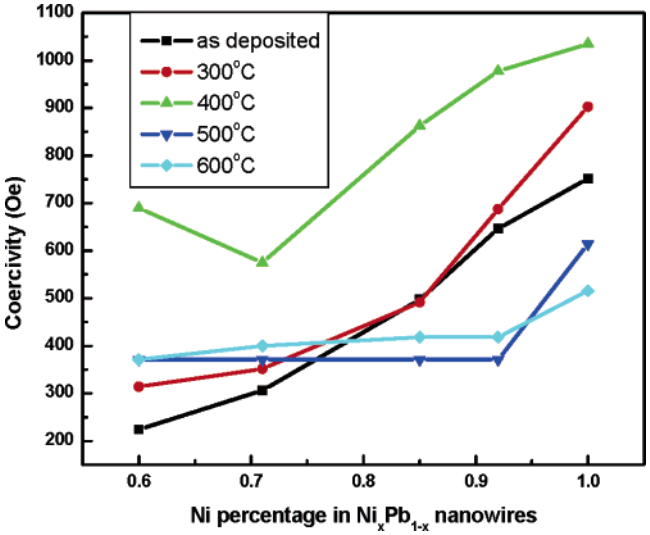

Figure 6. Coercivity vs annealing temperature with the applied field of 10 kOe.

before annealing and to increase by annealing (see the Supporting Information).

The hysteresis loops of the as-deposited samples with the external field perpendicular (⊥) and parallel (||) to the sample

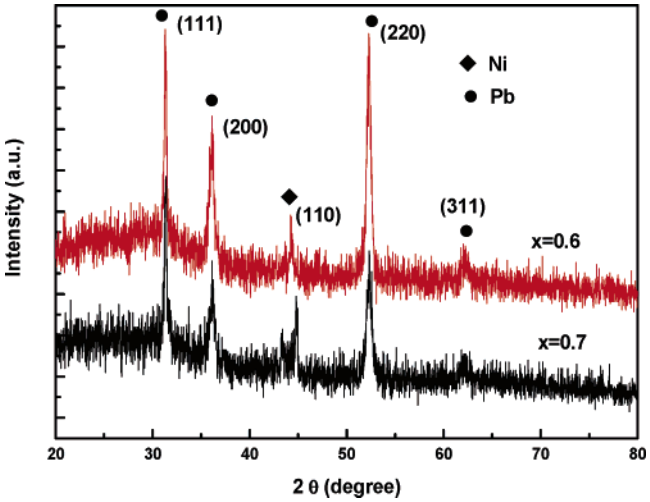

Figure 7. XRD patterns of the $Ni_{0.7}Pb_{0.3}$ and $Ni_{0.6}Pb_{0.4}$ nanowires annealed under the magnetic field.

plane at room temperature are measured. As one can see, the typical magnetic anisotropy behavior can be observed for the as-deposited Ni_xPb_{1-x} nanowire arrays (see Figure 5a). The coercivity and squareness with the fields applied parallel to the axis of nanowire arrays are much larger than those with the fields applied perpendicular to the nanowire arrays. We all know that the magnetostatic vector prefers to lie along the wire axis in order to reduce the magnetostatic energy. Hence, the nanoarrays have a direction of magnetization along the axis of the nanowires. Figure 5b shows the hysteresis loops of the as-deposited Ni_xPb_{1-x} ($0.60 < x < 1.0$) nanowire arrays with the diameter of about 20 nm. The external field is applied parallel to the long axes of the nanowires. It should be noted that $Hc\perp$ rapidly decreases as Pb content increases. The maximum value of approximately 751 Oe at the position of $x = 1$ (pure Ni nanowires) is observed. It is well-known that the crystallographic structure, chemical composition, diameter of the nanowires, and the aspect ratio effect the magnetic parameters such as *Hc* and *Ms*. In our samples, the chemical composition plays a key role in controlling the magnetic properties because the large influence of the nonmagnetic properties of the crystalline Pb phase which are formed in the nanowires deposited. From the Supporting Information, one can see that the crystallite size decreases with *x* increasing. The small crystallite size exhibits a relatively large negative K_1, causes a high *Hc* due to the magnetocrystallization anisotropy.

To study the annealing effects on Ni_xPb_{1-x} nanowires, all samples are annealed at different temperatures. The effect of annealing temperature on $Hc\perp$ measured at room temperature is shown in Figure 6 for all the Ni_xPb_{1-x} nanowires ($x = 0.60-1.0$). It is found that $Hc\perp$ of all samples have increased after annealing. As annealing temperature increases from 300 to 600

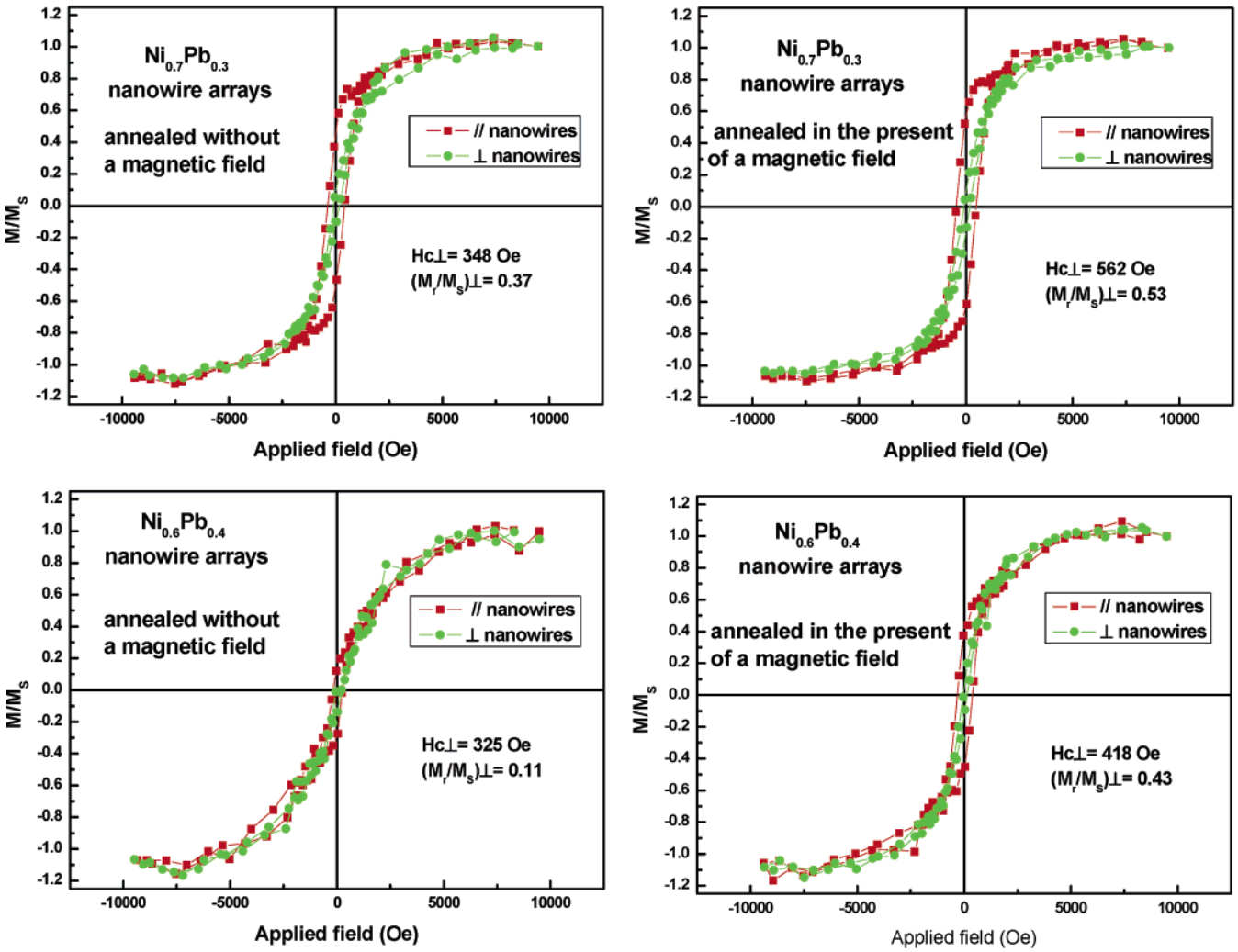

Figure 8. *M*−*H* loops of the $Ni_{0.7}Pb_{0.3}$ and $Ni_{0.6}Pb_{0.4}$ nanowire arrays annealed with and without the magnetic field measured in a magnetic field parallel and perpendicular to nanowires at room temperature.

°C, it is obviously found that the coercivity goes through a maximum t 400 °C. For annealed Ni_xPb_{1-x} nanowire arrays, the maximum coercivity is found to be 977.5 Oe at the position of $x = 1$ (pure Ni nanowires). The mechanism of this phenomenon is proposed as follows. First, the as-deposited Ni_xPb_{1-x} nanowires with a lower degree of crystallinity have a number of defects and high intrinsic stress due to the rapid AC electrodeposition; this will reduce the *Ms* in the as-deposited samples, and the anisotropy induced by stress may compete directly with shape anisotropy, which will decrease the coercivity and squareness. Thermal annealing relieves the internal stress, and a high degree of crystallinity is obtained. So the *Ms* of annealed samples is higher than its as-deposited state, and high coercivity is expected. Second, above 600 K (the Pb melting point), the samples transfer to liquid Pb and solid Ni, resulting in the possible existence of ferromagnetically interaction of Ni-rich particles or clusters. And some of the Pb atoms may act as defects and prevent the movement of the domain wall; then the coercivity will be improved in the samples. However on, further annealing above 500 °C, internal stress will increase and the alumina will distort. The pore of the AAO template will deviate from its original place, and the shape anisotropy will drop down. Furthermore, the number of ferromagnetically interacting particles increases slightly with increasing the annealing temperature above 500 °C, which will reduce $Hc\perp$. Unlike the Co−Pb alloy metastable phase nanowires reported previously,[14] the maximum $Hc\perp$ appears on the transformation temperature of the metastable phase (600 °C).

We have analyzed the crystal structure of the two heat-treated samples which were annealed under the magnetic field. The XRD patterns of the $Ni_{0.7}Pb_{0.3}$ and $Ni_{0.6}Pb_{0.4}$ nanowires annealed under magnetic field are shown in Figure 7. In comparison with Figure 4, the dominating peak of Pb is not the same as that of samples annealed in H_2, and the relative intensities of Pb peaks are much higher than those of Ni. It is clear that the magnetic field annealing enhances the phase separation.

Parts a and b of Figure 8 present the typical $M-H$ loops of the heat-treated $Ni_{0.7}Pb_{0.3}$ and $Ni_{0.6}Pb_{0.4}$ nanowire arrays measured at room temperature after annealing with and without the magnetic field. The $Hc\perp$ and squareness (M_r/M_s) for the annealed $Ni_{0.7}Pb_{0.3}$ and $Ni_{0.6}Pb_{0.4}$ nanowires in the presence of the applied field are 562 Oe, 0.53 and 418 Oe, 0.43, respectively. The perpendicular coercivity and squareness are much higher than that of the annealed two samples without the applied field. It should be noted that the coercivity and squareness with the fields applied perpendicular to the AAO planes are larger than those with the fields applied parallel to the AAO planes for all the samples, indicating that the nanoarrays possess a distinctive magnetic anisotropy along the nanowire direction. This direction is the same as the direction of the magnetic field during the annealing. For the magnetically annealed samples, the enhanced magnetic properties such as *Hc* and M_r/M_s in hysteresis loops clearly show magnetic anisotropy which can be attributed to the alignment of the grains. The easy axis of magnetization of the grains annealed in the magnetic field has a higher possibility to align along the nanowires. According to the nonmagnetic annealing process under the same annealing conditions for a longer period of time, the equilibrium phases may be reached. However, the mechanisms of magnetic field annealing still require further research work. Extensive studies are under investigation in our laboratory.

Conclusion

In conclusion, Ni_xPb_{1-x} nanowire arrays were successfully prepared by AC electrodeposition with AAO as template. The microstructure and magnetic properties of Ni_xPb_{1-x} nanowire arrays influence on Ni content and annealing were investigated. The structure of the Ni−Pb nanostructures is observed by TEM and XRD to be polycrystalline. Magnetic measurements show that the $Hc\perp$ and M_r/M_s of the Ni_xPb_{1-x} nanowires increases with x increasing before and after annealing. The magnetic properties enhanced for the annealed samples in the presence of a magnetic field.

Acknowledgment. This work was supported by the Project No. 50171033 of National Natural Science Foundation of China, the National Key Project of Fundamental Research (973, Grant No. G 1999064508), and the Scientific Research Foundation for the Enrollment Scholars of NUAA (Grant No. S0418-062).

Supporting Information Available: The crystal sizes of Ni_xPb_{1-x} nanowires before and after annealing from XRD data using the Scherrer equation. This material is available free of charge via the Internet at http://pubs.acs.org.

References and Notes

(1) Tonucci, R. J.; Justus, B. L.; Campillo, A. J.; Ford, C. E. *Science* **1992**, *258*, 783.

(2) Whitney, T. W.; Jiang, J. S.; Searson, P. C.; Chien, C. L. *Science* **1993**, *261*, 1316.

(3) Dubois, S.; Marchal, C.; Beuken, J. M.; Piraux, L. *Appl. Phys. Lett.* **1997**, *70*, 396.

(4) Guo, Y. G.; Wan, L. J.; Zhu, C, F.; Yang, D. L.; Chen, D. M.; Bai, C. L. *Chem. Mater*. **2003**, *15*, 664.

(5) Dubois, S.; Beuken, J. M.; Piraux, L.; Duvail, J. L.; Fret, A.; George, J. M.; Maurice, J. L. *J. Magn. Magn. Mater.* **1997**, *165*, 30.

(6) Blondel, A.; Meier, J. P.; Doudin, B.; Ansermet, J. P. *Appl. Phys. Lett*. **1994**, *65*, 3019.

(7) Martin, C. R. *Scienc*e **1994**, *266*, 1961.

(8) Zhou, P. H.; Xue, D. S.; Luo, H. Q.; Yao, J. L.; Shi, H. G. *Nanotechnology* **2004**, *15*, 27.

(9) Sellmyer, D. J.; Zheng, M.; Skomski, R. *J. Phys.: Condens. Matter* **2001**, *13*, R433.

(10) Yang, S. G.; Zhu, H.; Ni, G.; Yu, D. L.; Tang, S. L.; Du, Y. W. *J. Phys. D: Appl. Phys.* **2000**, *33*, 2388.

(11) Yang, S. G.; Zhu, H.; Yu, D. L.; Jin, Z. Q.; Tang, S. L.; Du, Y. W. *J. Magn. Magn. Mater*. **2000**, *222*, 97.

(12) (a) Su, H. L.; Ji, G. B.; Tang, S. L.; Li, Z.; Gu, B. X.; Du, Y. W. *Nanotechnology* **2005**, *16*, 429. (b) Tang, S. L.; Chen, W.; Lu, M.; Yang, S. G.; Zhang, F. M.; Du, Y. W. *Chem. Phys. Lett.* **2004**, *384*, 1. (c) Chen, W.; Tang, S. L.; Lu, M.; Du, Y. W. *J. Phys.: Condens. Matter* **2003**, *15*, 4626.

(13) Chen, W.; Li, Z.; Ji, G. B.; Tang, S. L.; Lu, M.; Du, Y. W. *Solid State Commun.* **2005**, *133*, 235.

(14) (a) Ji, G. B.; Tang, S. L.; Gu, B. X.; Du, Y. W. *J. Phys. Chem. B* **2004**, *108*, 8862. (b) Ji, G. B.; Tang, S. L.; Chen, W.; Gu, B. X.; Du, Y. W. *Solid State Commun.* **2004**, *132*, 289.

(15) (a) Pan, H.; Liu, B. H.; Yi, J. B.; Poh, C.; Lim, S.; Ding, J.; Feng, Y. P.; Huan, C.; Lin, J. Y. *J. Phys. Chem. B* **2005**, *109*, 3094. (b) Meng, G. W.; Cao, A. Y.; Cheng, J. Y.; Vijayaraghavan, A.; Jung, Y. J.; Shima, M.; Ajayan, P. M. *J. Appl. Phys.* **2005**, *97*, 064303. (c) Melle, S.; Menendez, J. L.; Armelles, G.; Navas, D.; Vazquez, M.; Nielsch, K.; Wehrspohnb, R. B.; Gosele, U. *Appl. Phys. Lett.* **2003**, *83*, 4547.

(16) (a) Adeyeye, A. O.; White, R. L. *J. Appl. Phys.* **2004**, *95*, 2025. (b) Qin, D. H.; Wang, C. W.; Sun, Q. Y.; Li, H. L. *Appl. Phys. A: Mater. Sci. Process.* **2002**, *74*, 761.

(17) (a) Chu, S. Z.; Inoue, S.; Wada, K.; Kanke, Y.; Kurashima, K. *J. Electrochem. Soc*. **2005**, *152*, C42. (b) Chu, S. Z.; Inoue, S.; Wada, K.; Kurashima, K. *J. Phys. Chem. B* **2004**, *108*, 5582. (c) Huang, Y. H.; Okumura, H.; Hadjipanayis, G. C.; Weller, D. *J. Appl. Phys.* **2002**, *91*, 6869.

(18) (a) Zhang, H. M.; Guo, Y. G.; Wang, L. J.; Bai, C. L. *Chem. Commun.* **2003**, *24*, 3022. (b) Wang, C. Z.; Meng, G. W.; Fang, Q. Q.; Peng, X. S.; Wang, Y. W.; Fang, Q.; Zhang, L. D. *J. Phys. D: Appl. Phys.* **2002**, *35*, 738.

(19) (a) Yuan, X. Y.; Wu, G. S.; Xie, T.; Lin, Y.; Zhang, L. D. *Nanotechnology* **2004**, *15*, 59. (b) Chiriac, H.; Moga, A. E.; Urse, M.; Paduraru, I.; Lupu, N. *J. Magn. Magn. Mater*. **2004**, *272−276*, 1678.

(20) Xue, D. S.; Shi, H. G. *Nanotechnology* **2004**, *15*, 1752.

(21) Blythe, H. J.; Fedosyuk, V. M.; Kasyutich, O. I.; Schwarzacher, W. *J. Magn. Magn. Mater.* **2000**, *208*, 251.

(22) Fedosyuk, V. M.; Kasyutich, O. I.; Schwarzacher, W. *J. Magn. Magn. Mater.* **1999**, *198*−*199*, 246.

(23) (a) Wang, Y. W.; Zhang, L. D.; Meng, G. W.; Peng, X. S.; Jin, Y. X.; Zhang, J. *J. Phys. Chem. B* **2002**, *106*, 2502. (b) Wang, Y. W.; Meng, G. W.; Liang, C. H.; Wang, G. Z.; Zhang, L. D. *Chem. Phys. Lett.* **2001**, *339*, 174. (c) Wang, Y. W.; Wang, G. Z.; Wang, S. X.; Gao, T.; Sang, H.; Zhang, L. D. *Appl. Phys. A: Mater. Sci. Process.* **2002**, *74*, 577.

(24) (a) Nielsch, F.; Muller, F.; Li, A.-P.; Gosele, U. *Adv. Mater.* **2000**, *12*, 582. (b) Chu, S. Z.; Wada, K.; Inoue, S.; Todoroki, S. *Chem. Mater.* **2002**, *14*, 4595. (c) Chu, S. Z.; Wada, K.; Inoue, S.; Todoroki, S. *Electrochim. Acta* **2003**, *48*, 3147.

(25) Wagner, C. D.; Riggs, W. M.; Davis, L. E.; Moulder, J. F.; Muilenberg, G. E. *Handbook of X-ray Photoelectron Spectroscopy*; Perkin-Elmer Corporation: Eden Prairie, MN, 1979; pp 81 and 144.

(26) (a) Kim, J. H.; Ahn, J. S.; Kim, J.; Park, M. S.; Lee, S. I.; Choi, E. J.; Oh, S.-J. *Phys. Rev. B: Condens. Matter. Mater. Phys.* **2002**, *66*, 172507. (b) Yu, G. H.; Zeng, L. R.; Zhu, F. W.; Chai, C. L.; Lai, W. Y. *J. Appl. Phys.* **2001**, *90*, 4039.